https://doi.org/10.15407/ujpe71.3.197

H.N. QASIM, F.H. AL-KHUDAIR

Department of Physics, College of Education for Pure Sciences,
University of Basrah
(Basrah, Iraq; e-mail: falih9@gmail.com)

INVESTIGATION OF THE X(5)-STRUCTURE IN EVEN-EVEN RARE-EARTH Sm–Os NUCLEI IN THE $N \approx 90$ REGION

Bands structure and nuclear shape in the $N \approx 90$ region are investigated using the interacting boson model. The energy levels and the energy ratios are investigated. We have studied the ratio $\delta E(J^-)/E(2_1^+)$ versus the mass number for the $J^- = 1^-$ to 11^- states. The ratio $E(J_i^+)/E(2_1^+)$ of the yrast bands versus angular momentum (J_i^+) has been calculated. The ^{152}Sm, ^{154}Gd and ^{160}Er nuclei have a rotational SU(3) character, while the ^{156}Dy, ^{170}W, and ^{176}Os nuclei reflect the X(5) character. To investigate the shape evolution, the potential energy surface as a function of β_2 and β_3 are plotted. The obtained results are compared with available empirical data. The results are in general good agreement for energy spectra, while they show reasonable agreement for other calculations or at least their overall trend.

K e y w o r d s: energy level, critical-point symmetry, boson model, mixing ratio.

1. Introduction

Critical point symmetries X(5) and E(5) [1, 2] which describe the nuclear structure of the nuclei at points of shape phase transitions within the symmetry triangle of the IBM. The nuclear structure of the rare-earth isotopes [3–5] has been examined previously both experimentally and theoretically [6–8]. Zhang *et al.* [9] obtained the critical behavior from spherical to axially deformed shapes for some rare-earth nuclei, in the space of two control parameters using the IBM. McCutchan *et al.* [10] examined the connection between a geometric approach and the X(5) solution. Zamfir *et al.* [11] compared empirical energies with interacting boson model (IBM) calculations for Gd–Hf isotopes. The authors plotted the symmetry triangle with an accurate location of the phase transition regions for the $N = 82$–104 nuclei. Gupta [12] considered the Davydov–Filippov model and performed a systematic analysis of the spectral features and electric transition probabilities of the $(\gamma < 20°)$ $(A \sim 160)$ deformed isotopes. Lee [13] investigated electromagnetic transitions between low-lying levels in $^{148-154}$Sm nuclei within the IBM-2 framework. The nuclear shape deformation parameters β and γ for $Z = 50$–82 have been studied using the asymmetric rotor model of Davydov–Filippov [14]. The effect of the $Z = 64$ subshell on the energy spectrum was identified. Pahlavani and Dinan [15] have investigated the level densities of the deformed nuclei in the formwork of the back-shifted Fermigas model. According to their calculation, the pairing energy is not constant and changes with temperature.

The following are some of the aims of this study:

1) To study the structure of the levels scheme in even-even deformed nuclei.

Citation: Qasim H.N., Al-Khudair F.H. Investigation of the X(5)-structure in even-even rare-earth Sm–Os nuclei in the $N \approx 90$ region. *Ukr. J. Phys.* **71**, No. 3, 197 (2026). https://doi.org/10.15407/ujpe71.3.197.

Table 1. **Interaction parameters (in MeV) adopted in the present study. $\chi = -1.323$ and $A_2 = -0.003$ MeV were chosen for all isotopes**

Nuclei	No.	ε_d	a_1	a_2	a_3	a_4	ε_f	A_1	A_3
^{152}Sm	10	0.116	0.006	−0.014	0.030	0.099	0.050	0.030	−0.072
^{154}Gd	11	0.123	0.008	−0.014	0.032	0.098	0.080	0.024	−0.075
^{156}Dy	12	0.138	0.009	−0.011	0.003	−0.058	0.310	0.014	−0.095
^{160}Er	12	0.125	0.007	−0.013	0.001	−0.057	0.310	0.014	−0.095
^{170}W	11	0.157	0.009	−0.014	0.035	0.098	0.040	0.026	−0.075
^{176}Os	12	0.135	0.009	−0.011	0.002	−0.058	0.260	0.015	−0.095

Table 2. **IBM-2 Hamiltonian parameters used in the calculations of positive-parity states in MeV units. $\chi_\nu = \chi_\pi = -1.2$, $\kappa_{\pi\nu} = -0.06$ MeV, and C_ν^L $(L = 0, 2, 4) = 0.02$ MeV were chosen for all isotopes**

Nuclei	No.	ε_d	$\xi_1 = \xi_3$	ξ_2	$C_\pi^L(L = 0, 2, 4)$
^{152}Sm	10	0.48	0.44	0.12	−0.64, −0.07, −0.02
^{154}Gd	11	0.51	0.23	0.10	−0.58, −0.05, −0.04
^{156}Dy	12	0.51	0.32	0.11	−0.57, 0.25, −0.01
^{160}Er	12	0.51	0.30	0.10	−0.50, −0.18, 0.08
^{170}W	11	0.51	0.30	0.10	−0.77, −0.14, 0.42
^{176}Os	12	0.51	0.30	0.10	−0.85, −0.21, 0.08

2) To investigate the probability of electric and magnetic transitions, as well as the mixing ratio.

3) To determine the positions of the symmetry and mixed-symmetry states.

2. The Model

With s- and d-bosons, the general model Hamiltonian is written as follows [16]:

$$H = \sum_{i=1}^{N} \varepsilon_i + \sum_{i>j}^{N} V_{ij}, \tag{1}$$

where ε_i and V_{ij} are the single-boson energies and the interaction between two bosons. In the multipole form, it can be written as follows [17, 18]

$$H_{sd} = \varepsilon_d \hat{n_d} + a_0 P^\dagger \cdot P + a_1 \hat{L} \cdot \hat{L} + a_2 \hat{Q} \cdot \hat{Q} + \\ + a_3 \hat{T}_3 \cdot \hat{T}_3 + a_4 \hat{T}_4 \cdot \hat{T}_4, \tag{2}$$

where ε_d, $\hat{n}_d$, $P^\dagger$, $\hat{L}$, $\hat{Q}$, $\hat{T}_r$ are the d-boson energy, the total number of d-bosons, the pairing, the quadrupole, the octupole ($r = 3$) and the hexadecapole ($r = 4$) operator, respectively. The description of the band structure of even-even nuclei has been performed within the formwork of the IBM-2 [19–21]. The Hamiltonian used in the present work is denoted as follows [22, 23]

$$H = H_\pi + H_\nu + H_{\pi\nu} \tag{3}$$

and

$$H = \varepsilon_d(\hat{n}_{d\nu} + \hat{n}_{d\pi}) + k_{\pi\nu}\hat{Q}_\nu \cdot \hat{Q}_\pi + \hat{V}_{\nu\nu} + \hat{V}_{\pi\pi} + \hat{M}_{\nu\pi}, \tag{4}$$

where ε_d, and $n_{d\rho}$ are the energy and the number of d-boson, respectively. The $k_{\pi\nu}\hat{Q}_\nu \cdot \hat{Q}_\pi$ term represents the quadrupole interaction. The quadrupole operator is written as:

$$\hat{Q}_\rho = (d_\rho^\dagger s_\rho + s_\rho^\dagger \tilde{d}_\rho)^{(2)} + \chi_\rho (d_\rho^\dagger \tilde{d}_\rho)^{(2)}, \tag{5}$$

$V_{\pi\pi}$ and $V_{\nu\nu}$ represent interaction between similar bosons, where

$$\hat{V}_{\rho\rho} = \frac{1}{2} \sum_{L=0,2,4} C_\rho^{(L)} [d_\rho^\dagger d_\rho^\dagger]^{(L)} \cdot [\tilde{d}_\rho \tilde{d}_\rho]^{(L)}. \tag{6}$$

The $\hat{M}_{\nu\pi}$ is the Majorana term, is expressed as follows:

$$\hat{M}_{\nu\pi} = \frac{1}{2}\xi_2 [s_\nu^\dagger d_\pi^\dagger - d_\nu^\dagger s_\pi^\dagger]^{(2)} \cdot [s_\nu \tilde{d}_\pi - \tilde{d}_\nu s_\pi]^{(2)} - \\ - \sum_{k=1,3} \xi_k [d_\nu^\dagger d_\pi^\dagger]^{(k)} \cdot [\tilde{d}_\nu \tilde{d}_\pi]^{(k)} \tag{7}$$

and it only affects on the energy of the mixed-symmetry states [24, 25].

3. Results and Discussion

3.1. Positive-parity states

In the present study, the parameters used in IBM-1 and IBM-2 are shown in Tables 1 and 2, respectively. To determine the energy spectra of nuclei under study, the ε_d and $\kappa_{\pi\nu}$ parameters were chosen

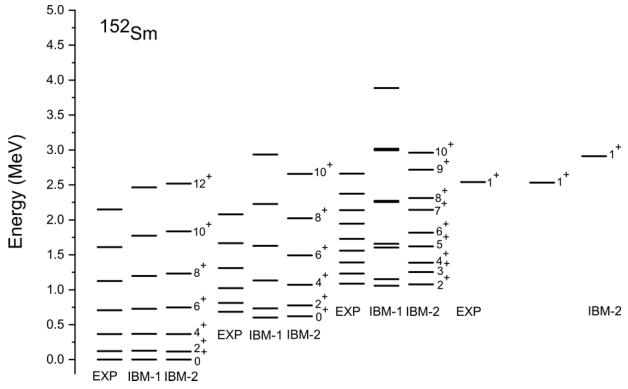

Fig. 1. The energy spectrum calculated in the boson model and the empirical data [26] of the ^{152}Sm isotope

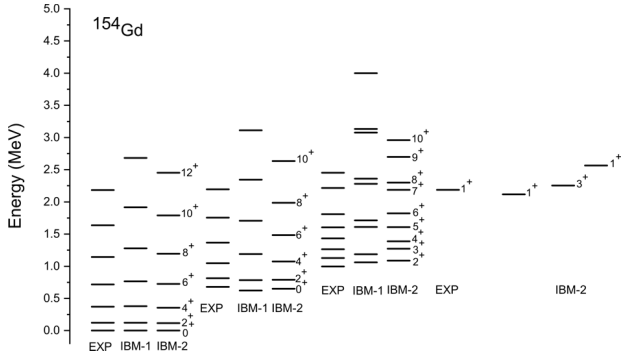

Fig. 2. The energy spectrum calculated in the boson model and the empirical data [26] of the ^{154}Gd isotope

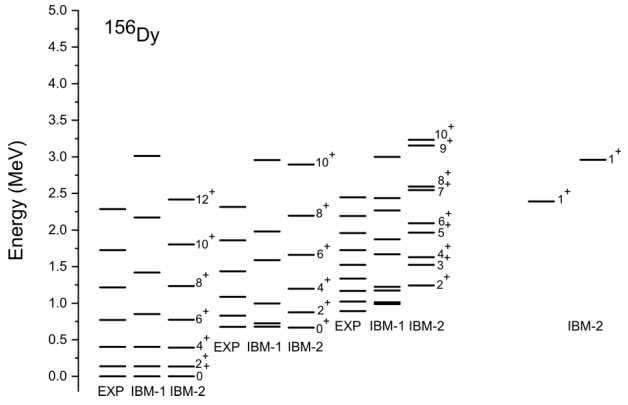

Fig. 3. The energy spectrum calculated in the boson model and the empirical data [26] of the ^{156}Dy isotope

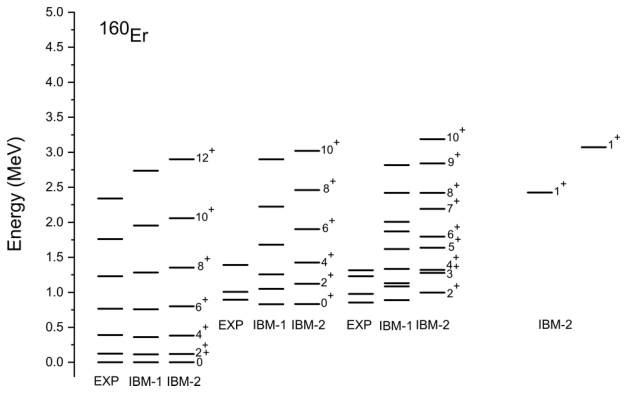

Fig. 4. The energy spectrum calculated in the boson model and the empirical data [26] of the ^{160}Er isotope

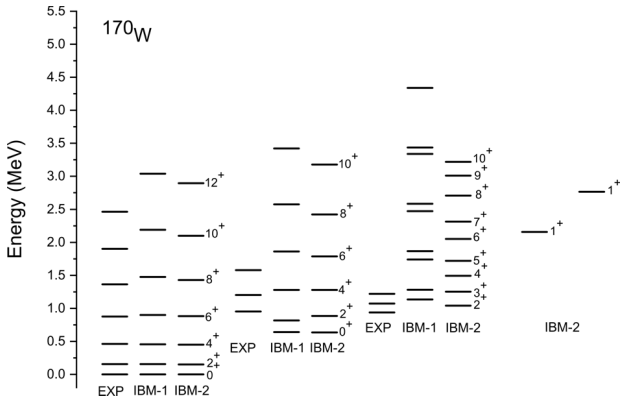

Fig. 5. The energy spectrum calculated in the boson model and the empirical data [26] of the ^{170}W isotope

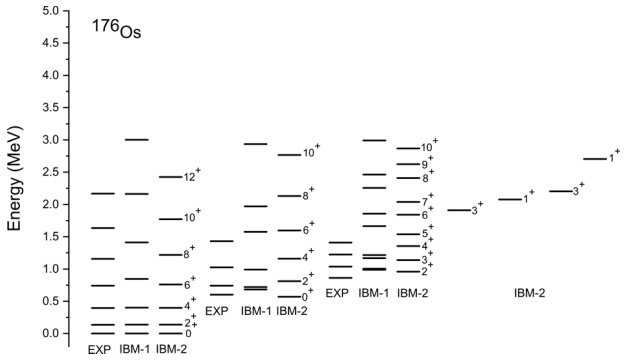

Fig. 6. The energy spectrum calculated in the boson model and the empirical data [26] of the ^{176}Os isotope

to fit the experimental low-lying energies as closely as possible. The values of χ_π and χ_ν were kept constant at (-1.2). The values of $\kappa_{\pi\nu}$ and $C_\nu^L (L = 0, 2, 4)$ were also kept fixed along the isotopic chain with -0.06 and 0.02, respectively, as shown in Table 2. In Figs. 1–6, the obtained results are presented together with the relevant experimental data. Examination of these figures shows that the model calculations agree with the experimental results, in particular, 0_2^+ states (two-phonon states). For the ^{152}Sm isotope,

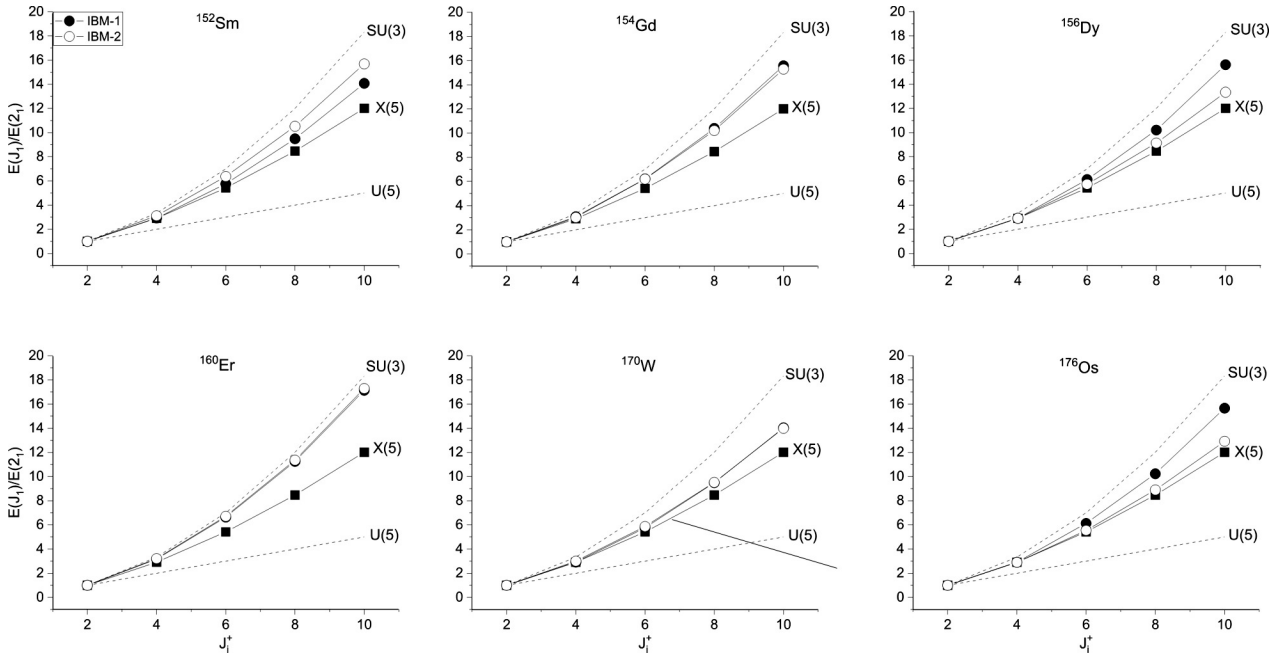

Fig. 7. The values of the $E(J_i^+)/E(2_1^+)$ for the yrast bands of even-even ^{152}Sm, ^{154}Gd, ^{156}Dy, ^{160}Er, ^{170}W and ^{176}Os nuclei as well as the X(5), U(5) and SU(3) predictions

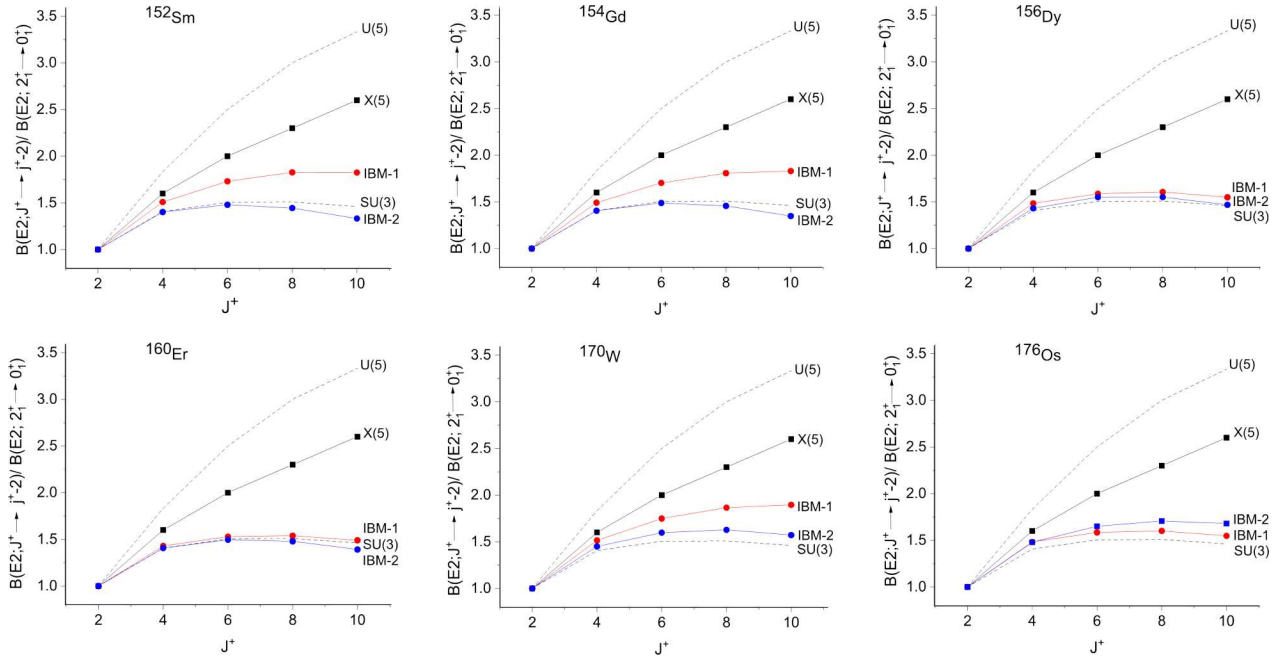

Fig. 8. The $B(E2; J_i^+ \to J_i^+ - 2)/B(E2; 2_1^+ \to 0_1^+)$, in comparison with the U(5), SU(3) limit values and the X(5) predictions

the g.s. band is well predicted. The $E(4_1^+)$ values are 0.366, 0.369 and 0.366 MeV and 6_1^+ state lies at 0.706, 0.727 and 0.746 MeV for Exp, IBM-1, and IBM-2 results, respectively. The energy of the 2_3^+ state was observed at 1.086 MeV in comparison with the IBM-1 and IBM-2 at 1.058, and 1.076 MeV, respectively. For

the ^{154}Gd isotope, Fig. 2 shows that the calculated states are all in good order and agree reasonably with the empirical data except for the γ-band states are higher than the experimental ones. The model results are successful in predicting the low-lying yrast states and β-band of the ^{156}Dy and ^{160}Er nuclei, as shown in Figs. 3 and 4. For the ^{170}W isotope, the theoretical and experimental energy levels are plotted in Fig. 5. As may be observed in Fig. 6, the results of the first and second versions of the IBM of $2_3^+, 3_1^+$ and 5_1^+ states are equal to (0.987, 0.958), (1.003, 1.137), and (1.215, 1.538) MeV. These values agree with the empirical ones at 0.863, 1.037, and 1.409 MeV, respectively. The $E(J_i^+)/E(2_1^+)$, with $J_i^+ = 4_1^+ - 10_1^+$ is illustrated in Fig. 7.

In Fig. 8, the $B(E2; J_i^+ \to J_i^+ - 2)/B(E2; 2_1^+ \to \to 0_1^+)$ are plotted together with the $X(5)$ predictions, as well as the U(5) and SU(3) limit values. Fig. 9 includes the $E4_1^+/E2_1^+$ and $E0_2^+/E2_1^+$ energy ratios in the IBM-2 prediction and the critical point symmetry X(5) value. The $R_{4/2}$ values are 3.13, 3.01, and 3.21 for ^{152}Sm, ^{154}Gd and ^{160}Er nuclei, respectively, which reflect the SU(3) limit. While the $R_{4/2}$ values are 2.91, 2.95 and 2.90 for ^{156}Dy, ^{170}W, and ^{176}Os nuclei, respectively, which indicate the X(5) character. In Fig. 10, the g.s. band levels of the Sm–Os nuclei, together with the corresponding experimental levels, are plotted. It can be shown in Fig. 11 that a change in the value of ζ_2 has a significant effect on the energy of the mixed-symmetry states.

3.2. Negative-parity states

By introducing the $L = 3$ boson (f-boson) into the *sd*-boson space, negative parity states for the Sm–Os nuclei have been explained within the *sdf* space model[29], where

$$N = n_s + n_d + n_f. \tag{8}$$

The Hamiltonian of the IBM-1 used to describe energy scheme is written as follows [29, 30]

$$H = H_{sd} + H_f + V_{sdf}, \tag{9}$$

the H_{sd} term describes the *sd* space, H_f is the f-boson Hamiltonian. The V_{sdf} term is written in the following form [18, 23, 31]

$$V_{sdf}^{\text{mult}} = A_1 L_d \cdot L_f + A_2 Q_d \cdot Q_f - A_3 Q^3 \cdot Q^3. \tag{10}$$

The results are presented together with corresponding experimental data in Figs. 12–14. For all nuclei,

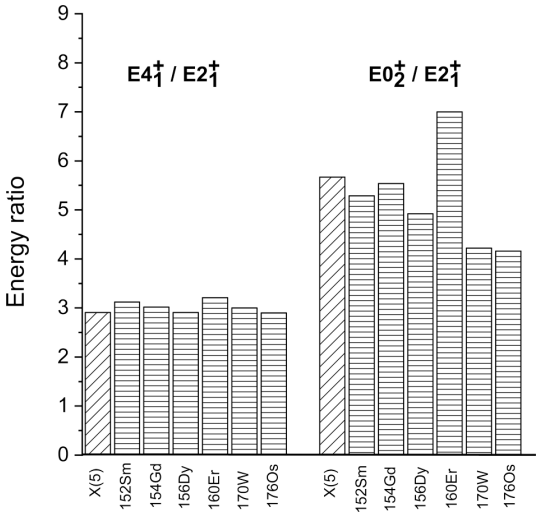

Fig. 9. $E4_1^+/E2_1^+$ and $E0_2^+/E2_1^+$ for the IBM-2 predictions and X(5) values

the position of the lower band with the 1_1^- head-band has been reproduced. Fig. 12 shows the comparison of the present calculation for the ^{152}Sm and ^{154}Gd isotopes with experimental data. For ^{152}Sm, the energies of the $(1_1^-, 3_1^-)$ states in the empirical and model results are (0.963, 1.041) and (0.965, 1.053) MeV, respectively. Minkov *et al.* [32] proposed the 1_1^- level at 0.853 MeV and the 3_1^- level at 0.922 MeV. Experimentally, the energy of the 5_1^- state is equal to 1.221 MeV, while the predicted energy is 1.224 MeV, whereas the energy values of the 7_1^- state are 1.505 and 1.540 MeV.

The energy of the 4_1^- state for the ^{154}Gd isotope is 1.559 and 1.501 MeV for empirical and model, respectively. For the ^{160}Er isotope, the $E(4_1^-)$, $E(6_1^-)$, and $E(8_1^-)$ levels are 1.632, 1.944, and 2.363 MeV, which are extremely close to observed ones at 1.638, 1.908, and 2.294 MeV as shown in Fig. 13, respectively. For the ^{176}Os isotope, $E(4_1^-) = 1.475$ and 1.474 MeV in the empirical and model results, respectively. The $E(2_1^-)$ state is calculated at 1.316 MeV as shown in Fig. 14. The variation in the energy of the negative-parity states is shown in Fig. 10.

4. Electromagnetic Transitions

The general electric quadrupole transition operator is written as follows [31]:

$$\hat{T}(E2) = e_{2SD}(s^\dagger \tilde{d} + d^\dagger s)^{(2)} + e_{2DD}(d^\dagger \tilde{d})^{(2)}, \tag{11}$$

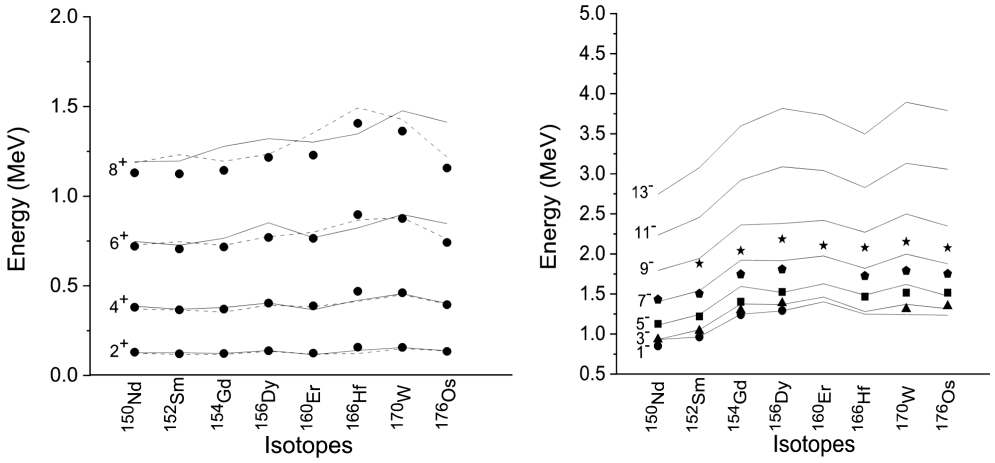

Fig. 10. The behavior of energy levels in IBM-1 (connected lines), IBM-2 (dotted lines) and the experimental data [26] (symbols), ^{150}Nd [27], ^{152}Sm, ^{154}Gd, ^{156}Dy, ^{160}Er,^{166}Hf [28], ^{170}W and ^{176}Os nuclei

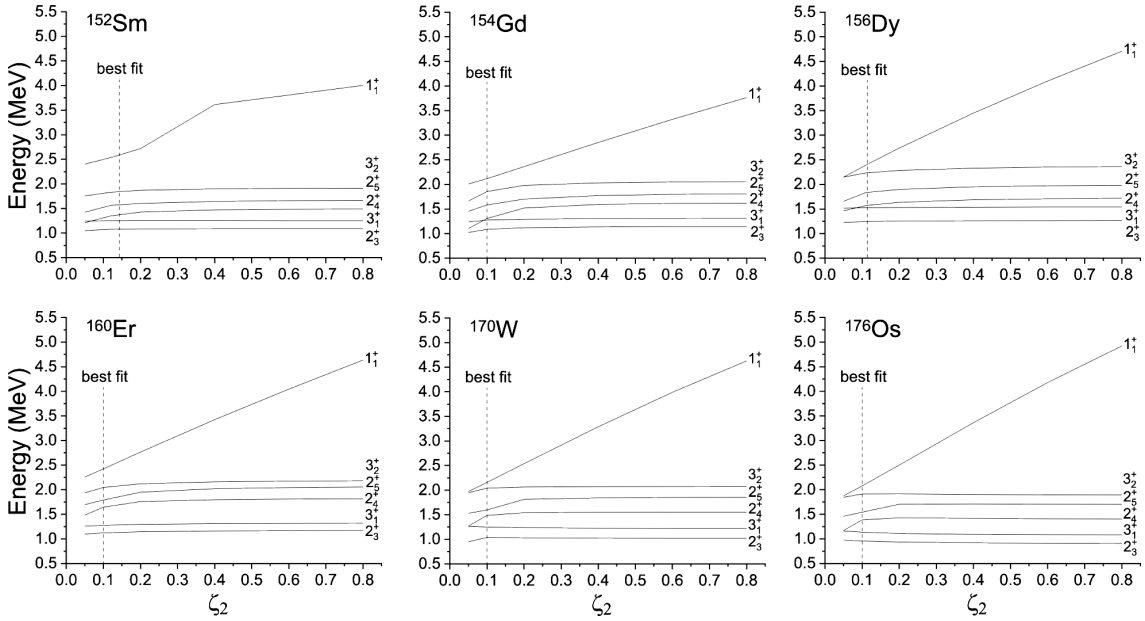

Fig. 11. Variation in energy-level values for the rare-earth Sm, Gd, Dy, Er, W and Os nuclei as a function of ζ_2

$$\hat{T}(E1) = e_{1Q}[\hat{T}(E2) \times (s^{\dagger}\tilde{f} + f^{\dagger}s)^{(3)}]^{(1)} + \\ + e_{1DF}(d^{\dagger}\tilde{f} + f^{\dagger}\tilde{d})^{(1)} \quad (12)$$

and

$$\hat{T}(E3) = e_{3Q}[\hat{T}(E2) \times (s^{\dagger}\tilde{f} + f^{\dagger}s)^{(3)}]^{(3)} + \\ + e_{3SF}(s^{\dagger}\tilde{f} + f^{\dagger}s)^{(3)} + e_{3DF}(d^{\dagger}\tilde{f} + f^{\dagger}\tilde{d})^{(3)}. \quad (13)$$

The $E2$ operator

$$T^{(E2)} = e_{\pi}Q_{\pi} + e_{\nu}Q_{\nu}, \quad (14)$$

and M1 operator is denoted by

$$T^{M1} = \sqrt{\frac{3}{4\pi}}(g_{\pi}L_{\pi}^{(1)} + g_{\nu}L_{\nu}^{(1)}) \quad (15)$$

$$T^{M1} = 0.77[(d^{\dagger}\tilde{d})_{\pi}^{(1)} - (d^{\dagger}\tilde{d})_{\nu}^{(1)}](g_{\pi} - g_{\nu}), \quad (16)$$

where e_{π}, e_{ν}, g_{π} and g_{ν} are the effective charge and g-factor for the proton and neutron boson, respectively. The $E2/M1$ mixing ratio is defined as follows [33]

$$\delta(E2/M1) = 0.835E_{\gamma}(\text{MeV})\Delta, \quad (17)$$

where

$$\Delta = \frac{\langle j_f \parallel T^{E2} \parallel Ji\rangle}{\langle J_f \parallel T^{M1} \parallel Ji\rangle}. \quad (18)$$

The $B(E2/M1)$ transition probability is defined as follows:

$$B(E2/M1\text{: } J_i \to J_f) =$$

$$= \frac{1}{2J_i+1} \mid \langle J_f \parallel T^{E2/M1} \parallel J_i\rangle \mid^2 . \quad (19)$$

For IBM-1 calculations, the effective boson charges e_{2SD} and e_{2DD} in the transition operator in Eq. (11) are adjusted to the experimental data of $B(E2; 2_1^+ \to \to 0_1^+)$. Table 3 includes the values of the e_{2SD} and e_{2DD} parameters. In IBM-2 calculations, for the magnetic transitions, we take $g_\nu = 0.12\mu_N$, $g_\pi = 0.85\mu_N$ for all nuclei. Table 4 displays the $B(E2)$ values calculated in (e^2b^2) for the Sm–Os nuclei. The experimental results are compared with the IBM results. From this table, one can see that the $B(E2)$ values of the $4_1^+ \to 2_1^+$ transition are equal to 1.009(105), 1.0478 and 0.9672 for the ^{152}Sm isotope in the (Exp, IBM-1 and IBM-2) results. As shown in Table 5, the $B(E2; J_i^- \to J_f^-)$ transition probabilities between the members of octupole bands are calculated.

The $B(E2; 11_1^- \to 9_1^-) = 1.0065(5032)$, 0.4955 e^2b^2 for the ^{170}W isotope in the (Exp, IBM-1) results, respectively. The $B(E1)$ and $B(E3)$ for ^{152}Sm, ^{154}Gd, ^{156}Dy, ^{160}Er, ^{170}W, and ^{176}Os nuclei were calculated as shown in Tables 6 and 7. The values of coefficients e_{1Q}, e_{1Df}, e_{3Q}, e_{3SF} and e_{3DF} are listed in Table 3, these values are estimated by fitting the observed $B(E1; 1_1^- \to 2_1^+)$ in the ^{152}Sm and ^{154}Gd, respectively. There is no experimental data for $B(E3)$.

The $B(M1)$ values are shown in Tables 8. We observed that the theoretical values of $B(M1; 1_1^+ \to 0_1^+)$ transition is larger than $B(M1; 1_1^+ \to 2_1^+)$ transition for all the nuclei under study, and these transitions

Table 3. **The values of (e_{2SD}, e_{2DD}) (in units of $e\ b$), (e_{1Q}, e_{1DF}) (in units of $e\ b^{1/2}$) and (e_{3Q}, e_{3SF}) (in units of $e\ b^{3/2}$), where $e_{1Df} = e_{3SF} = e_{3DF} = 0.0$**

$B(E\lambda)$	Parameter	^{152}Sm	^{154}Gd	^{156}Dy	^{160}Er	^{170}W	^{176}Os
$B(E2)$	e_{2SD}	0.196	0.189	0.278	0.254	0.182	0.296
	e_{2DD}	0.030	0.030	0.030	0.030	0.030	0.030
$B(E1)$	e_{1Q}	0.050	0.134	0.050	0.050	0.050	0.050
$B(E3)$	e_{3Q}	1.000	1.000	1.000	1.000	1.000	1.000

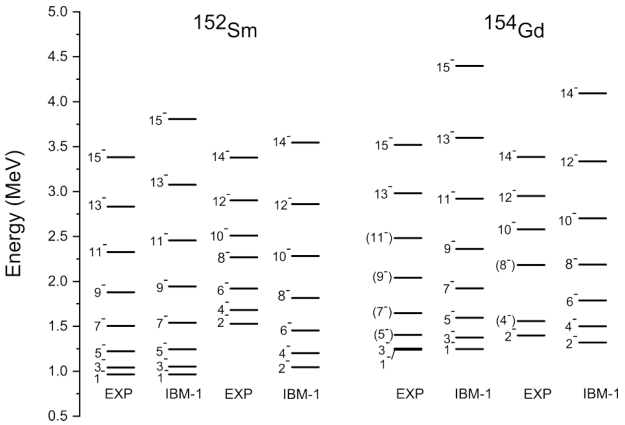

Fig. 12. Calculated and observed level schemes in the ^{152}Sm and ^{154}Gd isotopes

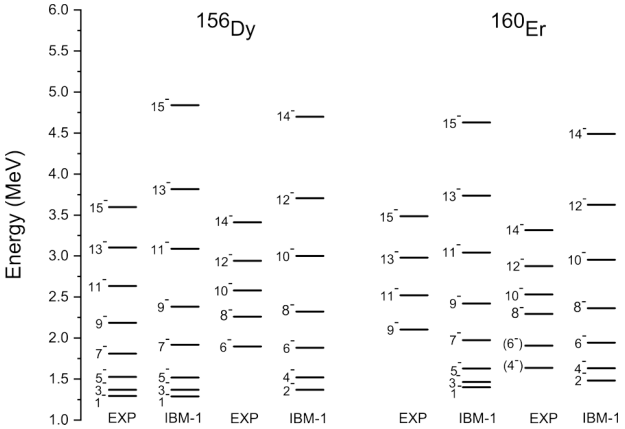

Fig. 13. Calculated and observed level schemes in the ^{156}Dy and ^{160}Er isotopes

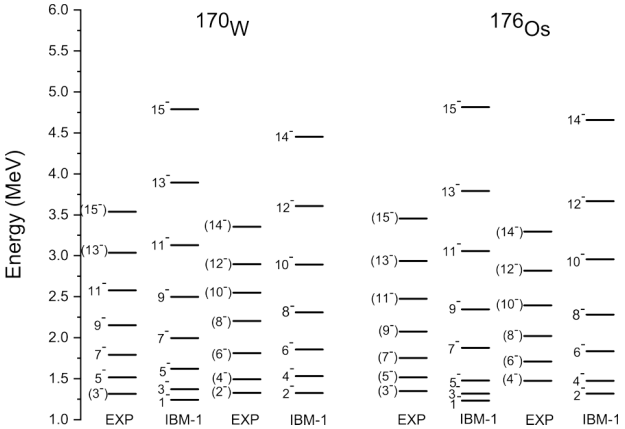

Fig. 14. Calculated and observed level schemes in the ^{170}W and ^{176}Os isotopes

Table 4. **The absolute $B(E2)$ values calculated in (e^2b^2), compared with the available experimental data [26]**

$J_i^+ \to J_f^+$	^{152}Sm			^{154}Gd			^{156}Dy		
	Exp	IBM-1	IBM-2	Exp	IBM-1	IBM-2	Exp	IBM-1	IBM-2
$2_1 \to 0_1$	0.698(77)	0.6946	0.6901	0.770(4)	0.7777	0.7521	0.748(84)	0.7445	0.7470
$4_1 \to 2_1$	1.009(105)	1.0478	0.9672	1.200(44)	1.1594	1.0572	1.220(119)	1.1048	1.0697
$6_1 \to 4_1$	1.156(19)	1.2024	1.0214	1.396(73)	1.3249	1.1191	1.316(64)	1.1813	1.1584
$8_1 \to 6_1$	1.411(19)	1.2693	0.9969	1.529(83)	1.4055	1.0964	1.401(39)	1.1951	1.1592
$10_1 \to 8_1$	1.512^{+168}_{-125}	1.2683	0.9198	1.764(19)	1.4228	1.0142	1.546(14)	1.1532	1.0980
$12_1 \to 10_1$		1.2050	0.8019		1.3829	0.8958	1.645(19)	1.0640	0.9933
$2_2 \to 0_1$	0.004(28)	0.0536	0.0003	0.004(34)	0.0508	0.0004		0.1275	0.0019
$2_2 \to 2_1$	0.027(19)	0.3831	0.0001	0.032(29)	0.3383	0.0003		0.0050	0.1346
$2_2 \to 4_1$	0.086(57)	0.0014	0.0009	0.096(78)	0.0018	0.0027		1.9886	0.0177
$2_3 \to 0_1$	0.013(19)	0.0354	0.0002	0.027(24)	0.0501	0.0008	0.035(39)	0.0591	0.0087
$2_3 \to 2_1$	0.041(42)	0.0146	0.0069	0.060(49)	0.0211	0.0063	0.046(59)	0.2986	0.0400
$3_1 \to 2_1$		0.1336	0.0006		0.1546	0.0015		0.1204	0.0145
$3_1 \to 2_2$		0.5674	0.0132		0.5600	0.0143		0.5742	0.0012
$5_1 \to 3_1$		0.6615	0.4368		0.7259	0.4811		0.4565	0.5143
	^{160}Er			^{170}W			^{176}Os		
$2_1 \to 0_1$	0.856(36)	0.8560	0.8327	0.693(16)	0.6953	0.6957	0.843(29)	0.8472	0.8189
$4_1 \to 2_1$	1.237(46)	1.2234	1.1712	1.001(11)	1.0536	1.0089		1.2511	1.2101
$6_1 \to 4_1$	1.351(77)	1.3095	1.2459	1.056(78)	1.2165	1.1112		1.3372	1.3502
$8_1 \to 6_1$	1.547(36)	1.3183	1.2318	1.062(279)	1.2977	1.1323		1.3525	1.3964
$10_1 \to 8_1$	1.495(36)	1.2754	1.1586	0.950(223)	1.3180	1.0938		1.3048	1.3751
$12_1 \to 10_1$		1.1915	1.0342		1.2835	0.9919		1.2046	1.2754
$2_2 \to 0_1$		0.1015	0.0006		0.0484	0.0001		0.1401	0.0012
$2_2 \to 2_1$		0.0256	0.0033		0.3627	0.0434		0.0064	0.0640
$2_2 \to 4_1$		0.0671	0.0024		0.0031	0.0565		0.1381	0.0742
$2_3 \to 0_1$		0.0520	0.0057		0.0387	0.0080		0.0711	0.0068
$2_3 \to 2_1$		0.2292	0.0093		0.0196	0.0156		0.3369	0.0169
$3_1 \to 2_1$		0.1096	0.0085		0.1332	0.0114		0.1332	0.0129
$3_1 \to 2_2$		0.7666	0.0007		0.5382	0.0707		0.6616	0.1631
$5_1 \to 3_1$		0.5209	0.5604		0.6705	0.4924		0.5151	0.6368

are the strongest. The $M1$ decay of 1_1^+ to 2_2^+ and 2_3^+ states are dominant for all isotopes. The mixing ratio $\delta(E2/M1)$ for the selected transitions are presented in Table 9. We observe that for the ^{176}Os isotope, the $\delta(3_1^+ \to 4_1^+)$ is equal to -2.9^{+5}_{-7} and -2.582 in the Exp and predicted values, respectively. The 3_1^+ state has dominant $M1$ decays to 2_1^+ with $\delta(E2/M1) = = -2.195$. The 3_2^+ state decays to 2_1^+ by dominant $M1$ with $\delta(E2/M1) = +1.157$, in the ^{170}W isotope.

5. The Energy Displacement $\delta E(J^-)$

We have studied the energy displacement $\delta E(J^-)$ to determine to identify wether the members of rotational bands are octupole-deformed or octupole-vibrational states. This distinction can be investigated by the quantity [34]

$$\delta E(J^-) = E(J^-) - \frac{E[(J+1)^+] + E[(J-1)^+]}{2}, \quad (20)$$

where $E(J-)$ denotes the excitation energies of odd-J^- yrast states, and $E((J \pm 1)+)$ denotes the excitation energies of even-J^+ yrast states. In Fig. 15, the calculated $\delta E(J^-)/E(2_1^+)$ values for the $J^- = 1^-$, $3^-, 5^-, 7^-, 9^-$ and 11^- states are shown. For the nuclei under investigation, the ratios $\delta E(J^-)/E(2_1^+)$ for each angular momentum are not equal to zero, indicating that they are octupole-deformed states.

6. Potential Energy Surface

The PES is very successful in describing the nuclear shape. Its values as a function of the deformation pa-

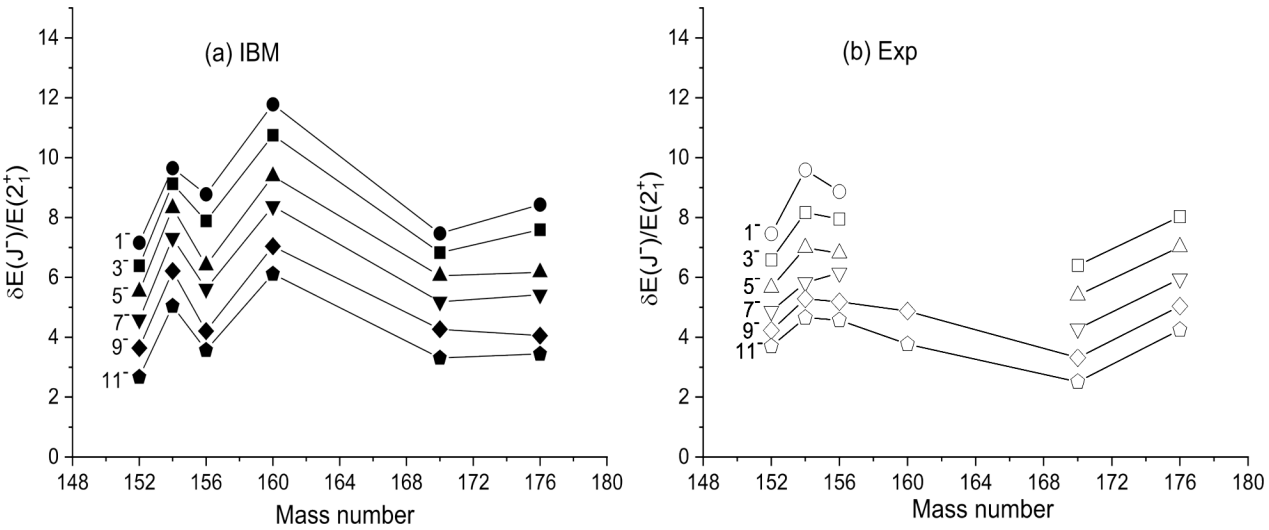

Fig. 15. The energy displacement $\delta E(J^-)$, normalized with respect to the 2_1^+ state, as a function of the mass number for the $J^- = 1^-, 3^-, 5^-, 7^-, 9^-$, and 11^- states

rameters β_2 and γ are given by [18]:

$$V(\beta_2,\gamma) = \frac{N_B}{1+\beta_2^2}(R_1+R_2\beta_2^2)+\frac{N_B(N_B-1)}{(1+\beta_2^2)^2}(R_3\beta_2^4 + \\ + R_4\beta_2^3\cos 3\gamma + R_5\beta_2^2 + R_6), \quad (21)$$

where β_2, γ and N_B represent the quadrupole deformation, asymmetry angle, and boson number. R_1 to R_6 are related to the Hamiltonian parameters. In Fig. 16, we display the contour plot of the PES for Sm–Os nuclei. The results show that these isotopes are deformed and exhibit rotational-like characteristics SU(3).

In Refs. [35–38], the quadrupole-octupole deformation energy surfaces in the quadrupole (β_2) and the octupole (β_3) shape variables in the boson system have been found for many isotopic chains. Where

$$V(\beta_2,\beta_3) = \frac{N_B}{1+\bar{\beta}_2^2+\bar{\beta}_3^2}(\acute{\epsilon_s} + \acute{\epsilon_d}\bar{\beta}_2^2 + \acute{\epsilon_f}\bar{\beta}_3^2) +$$

Table 5. **The calculated $B(E2)$ (in units of e^2b^2), the available experimental data [26] for $B(E2; 2_1^- \to 3_1^-)$ and $B(E2; 2_1^- \to 1_1^-)$ which are equal to 0.1204(0.0240) and 0.0067(0.0433) for the ^{152}Sm isotope, respectively and $B(E2; 11_1^- \to 9_1^-)$ is equal to 1.0065(5032) for the ^{170}W isotope**

$J_i^- \to J_f^-$	^{152}Sm	^{154}Gd	^{156}Dy	^{160}Er	^{170}W	^{176}Os
$3_1 \to 1_1$	0.2656	0.3258	0.0562	0.0891	0.2941	0.0563
$4_1 \to 2_1$	0.2608	0.3214	0.0271	0.0586	0.2765	0.0278
$5_1 \to 3_1$	0.3447	0.4083	0.0837	0.1314	0.3993	0.0834
$6_1 \to 4_1$	0.3324	0.3937	0.0671	0.1112	0.3794	0.0673
$6_1 \to 5_1$	0.0045	0.0415	0.0139	0.0218	0.0571	0.0137
$7_1 \to 5_1$	0.3581	0.4573	0.0923	0.1454	0.4522	0.0921
$8_1 \to 6_1$	0.3490	0.4361	0.0825	0.1302	0.4348	0.0823
$8_1 \to 7_1$	0.0010	0.0343	0.0099	0.0140	0.0409	0.0097
$9_1 \to 7_1$	0.3371	0.4847	0.1008	0.1532	0.4833	0.1003
$10_1 \to 8_1$	0.3315	0.4584	0.0882	0.1360	0.4612	0.0878
$10_1 \to 9_1$	0.0001	0.0269	0.0055	0.0087	0.0298	0.0054
$11_1 \to 9_1$	0.2890	0.4945	0.0988	0.1505	0.4955	0.0984
$13_1 \to 11_1$	0.2162	0.4858	0.0947	0.1428	0.4881	0.0941

Table 6. **The transition probabilities $B(E1)$ in $10^{-3}e^2b$ units compared with the experimental data [26]**

$J_i^- \to J_f^+$	^{152}Sm		^{154}Gd		^{156}Dy	^{160}Er	^{170}W	^{176}Os
	Exp	IBM	Exp	IBM	IBM	IBM	IBM	IBM
$3_1 \to 2_1$	0.149 (27)	0.002		3.178	1.750	1.698	0.492	1.761
$3_1 \to 2_2$		0.001		0.644	0.004	0.001	0.082	0.004
$1_1 \to 0_1$	0.106 (49)	0.005	0.889	1.185	1.720	1.630	0.199	1.721
$1_1 \to 0_2$		0.008	0.106	1.255	0.161	0.194	0.266	0.159
$1_1 \to 2_1$	0.195 (16)	0.141	0.898	0.889	0.112	0.126	0.052	0.114
$1_1 \to 2_2$	0.004 (26)	0.037	0.118	0.397	0.040	0.031	0.042	0.039
$2_1 \to 2_1$		0.118		1.386	0.633	0.701	0.176	0.064
$2_1 \to 2_2$		0.055		0.808	0.229	0.177	0.149	0.225
$5_1 \to 4_1$		0.001		5.540	1.746	1.751	0.809	1.758

Table 7. **The calculated values for the transition probabilities $B(E3)$ in e^2b^3 units for the Sm–Os nuclei**

$J_i^- \to J_f^+$	^{152}Sm	^{154}Gd	^{156}Dy	^{160}Er	^{170}W	^{176}Os	$J_i^- \to J_f^+$	^{152}Sm	^{154}Gd	^{156}Dy	^{160}Er	^{170}W	^{176}Os
$3_1 \to 0_1$	0.0013	2.8975	0.6244	0.9613	4.5097	0.6157	$2_1 \to 2_2$	0.0032	0.0137	0.1040	0.0553	0.0210	0.0983
$3_1 \to 0_2$	0.0001	0.0701	0.3988	0.3255	0.1017	0.3888	$2_1 \to 2_3$	0.0002	0.0021	0.2509	0.2752	0.0017	0.2599
$3_1 \to 2_1$	0.0135	3.1564	0.3912	0.4613	3.3041	0.3942	$4_1 \to 2_1$	0.0665	1.9956	0.9251	1.1970	3.7302	0.9138
$3_1 \to 2_2$	0.0005	0.0061	0.0340	0.0141	0.0045	0.0323	$4_1 \to 2_2$	0.0002	0.0043	0.0936	0.0446	0.0058	0.0876
$3_1 \to 4_1$	0.2354	1.7541	0.0121	0.0218	0.7675	0.0132	$4_1 \to 4_1$	0.7334	3.6796	0.0793	0.2016	3.6815	0.0858
$1_1 \to 2_1$	0.2227	5.4141	1.0192	1.4106	7.8320	1.0138	$5_1 \to 2_1$	0.0006	5.3508	0.9779	1.3273	6.6182	0.9706
$1_1 \to 2_2$	0.0016	0.0363	0.1077	0.0602	0.0543	0.1020	$5_1 \to 4_1$	0.0107	2.1644	0.0371	0.0838	1.5938	0.0394
$2_1 \to 2_1$	0.6864	2.9698	0.9869	1.3425	4.9208	0.9798							

Table 8. **The transition probabilities $B(M1)$ (in units for the μ_N^2) compared with the experimental data [26]**

$Ji^+ \to J_f^+$	^{152}Sm		^{154}Gd		^{156}Dy	^{160}Er	^{170}W	^{176}Os
	Exp	IBM	Exp	IBM	IBM	IBM	IBM	IBM
$2_2 \to 2_1$	0.0026(125)	0.00101	0.0002(268)	0.00206	0.00079	0.00136	0.00181	0.00130
$2_3 \to 2_1$	0.0002(537)	0.00024	0.0003(411)	0.00085	0.00332	0.00000	0.00431	0.00538
$2_4 \to 2_1$		0.00046		0.00129	0.00045	0.00959	0.00989	0.00792
$2_5 \to 2_1$		0.00020		0.00000	0.00240	0.00815	0.02354	0.01528
$2_5 \to 2_2$		0.00057		0.00233	0.00256	0.00000	0.01436	0.00301
$3_1 \to 2_1$		0.00005		0.00058	0.00259	0.00005	0.00139	0.00113
$3_1 \to 2_2$		0.00001		0.00000	0.00000	0.00000	0.00013	0.00059
$3_2 \to 2_1$		0.00001		0.00000	0.00033	0.00004	0.00059	0.00004
$3_2 \to 2_2$		0.00001		0.00050	0.00117	0.00006	0.00148	0.00057
$3_1 \to 4_1$	0.0004^{+107}_{-895}	0.00013		0.00093	0.00339	0.00003	0.00193	0.00174
$1_1 \to 0_1$		0.25907		0.30393	0.25276	0.30983	0.18863	0.18086
$1_1 \to 2_1$		0.15290		0.17981	0.14707	0.18496	0.11651	0.11333
$1_1 \to 2_2$		0.00698		0.00023	0.00008	0.00024	0.01176	0.01910
$1_1 \to 2_3$		0.08462		0.07550	0.13498	0.04672	0.05676	0.04562

Table 9. **Mixing ratios $\delta(E2/M1)$ in units of eb/μ_N compared with the available experimental data**

$Ji^+ \to J_f^+$	^{152}Sm		^{154}Gd		^{156}Dy	^{160}Er	^{170}W		^{176}Os	
	Exp	IBM	Exp	IBM	IBM	IBM	Exp	IBM	Exp	IBM
$2_2 \to 2_1$	$+19^{+5}_{-4}$	+0.169	+7.5(4)	+0.234	−2.371	−0.953		+3.250	-4.2^{+5}_{-6}	+3.549
$2_3 \to 2_1$	−9.3(6)	+4.264	−9.4(4)	+1.979	+2.181	−794.651		−1.240	$+11^{+0}_{-5}$	−1.079
$2_4 \to 2_1$		+2.231		+1.184	−1.499	+0.244		+0.063		−0.087
$2_5 \to 2_1$		+2.615		−642.968	+0.465	+0.007		−0.216		−0.350
$3_1 \to 2_1$		+3.206	−7.4(4)	+1.363	+1.747	−8.895	≤+15	−2.195	-9^{+3}_{-5}	−2.550
$3_2 \to 2_1$		−51.234		+381.561	+1.127	−0.300		+1.157		+1.736
$3_1 \to 4_1$	−6.5(3)	+5.634	−6.1(3)	+2.136	+1.655	−8.284		−2.080	-2.9^{+5}_{-7}	−2.582
$1_1 \to 2_1$		−0.510		−0.364	−0.503	−0.572		−1.181		−1.382
$1_1 \to 2_2$		−1.457		−4.643	−8.059	−5.626		+0.218		+0.272
$1_1 \to 2_3$		+0.118		−0.153	−0.242	−0.052		+0.062		+0.005
$1_2 \to 2_3$		−0.282		−0.222	+0.517	−0.541		+0.166		+0.081

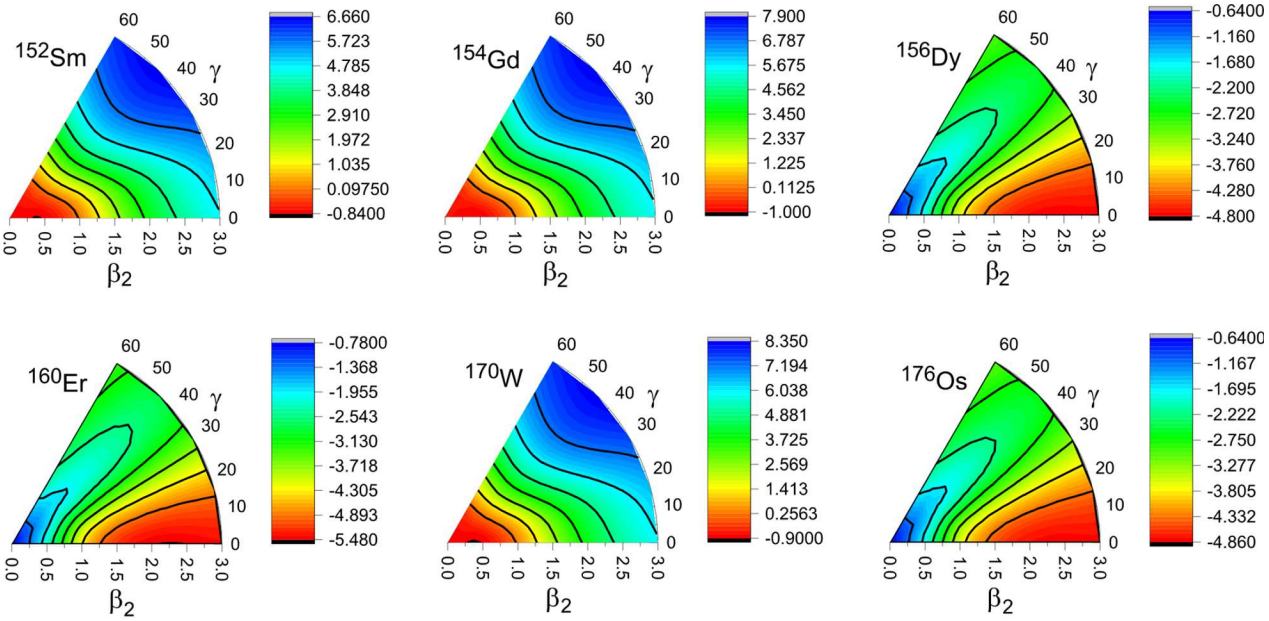

Fig. 16. The potential energy surface for the Sm–Os nuclei, within the deformation parameters: $0° \leq \gamma \leq 60°$ and $0 \leq \beta_2 \leq 3$

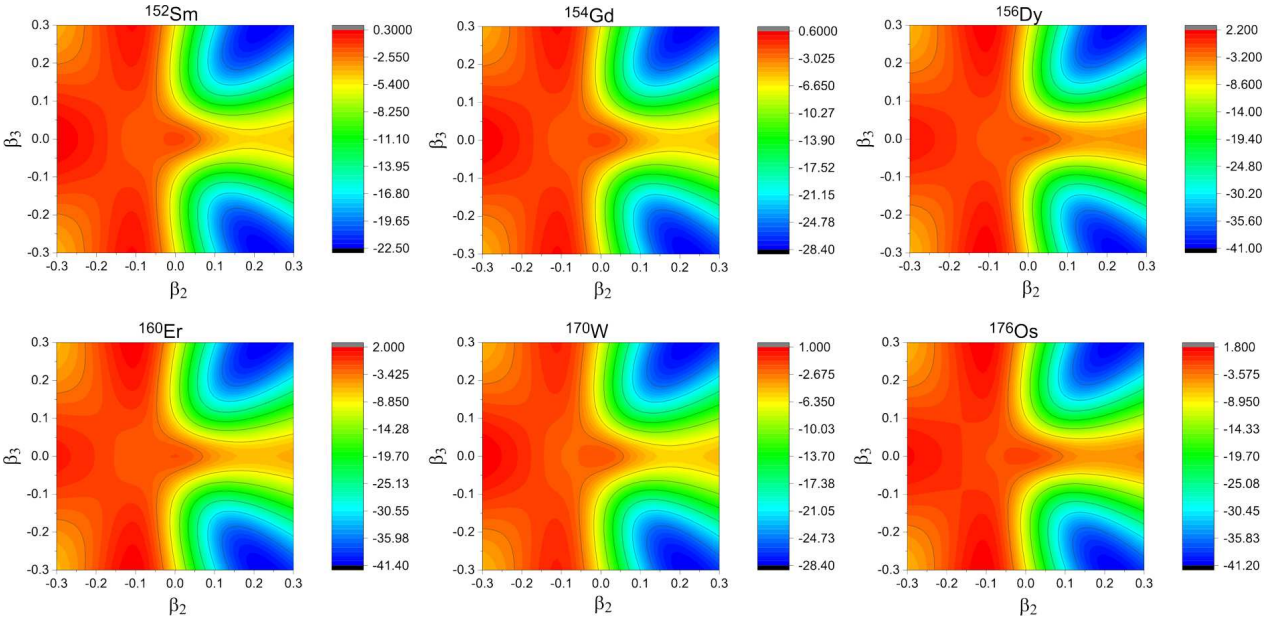

Fig. 17. The IBM potential energy surface for the Sm–Os nuclei in the (β_2, β_3) plane

$$+\frac{N_B(N_B-1)}{(1+\bar{\beta}_2^2+\bar{\beta}_3^2)^2}\left[\kappa_2\left(2\bar{\beta}_2-\sqrt{\frac{2}{7}}\chi_d\bar{\beta}_2^2-\frac{2}{\sqrt{21}}\chi_f\bar{\beta}_3^2\right)^2\right]+$$

$$+4\kappa_3(\bar{\beta}_3-\frac{2}{\sqrt{15}}\chi_3\bar{\beta}_2\bar{\beta}_3)^2, \qquad (22)$$

with

$$\epsilon_s' = 5\kappa_2, \quad \epsilon_d' = \varepsilon_d + 6\alpha + (1+\chi_d^2)\kappa_2,$$
$$\epsilon_f' = \varepsilon_f + \frac{5}{7}\kappa_2\chi_f^2, \qquad (23)$$

where $\alpha = a_0/2$, $k_2 = 2a_2$, $\chi_3 = \sqrt{5}\chi$ and $k_3 = A_3$. $\bar{\beta}$ is different from β [39]. The PES(β_2, β_3) are graphed in Fig. 17. For all isotopes, the PES is symmetric with respect to the $\beta_3 = 0$ axis. The quadrupole deformation shape becomes clear in these isotopes. The ground state has no octupole deformation.

7. Conclusion

In conclusion, the positive- and negative-parity bands of rare-earth Sm–Os nuclei have been studied. The results of the model suggest that the ^{156}Dy, ^{170}W, and ^{176}Os are good candidates for X(5) symmetry, but the ^{152}Sm, ^{154}Gd, and ^{160}Er are poor candidates for X(5) critical-point symmetry. The calculated ratio $R = \langle J \mid F^2 \mid J\rangle / F_{\max}(F_{\max}+1)$, which measures the F-spin of states, and the effect of the Majorana ζ_2 parameter on the energy levels. The results show that the 2_3^+, 2_4^+, and 2_5^+ are fully symmetric states, and the 1_1^+ state is the lowest mixed-symmetry state in all nuclei.

1. F. Iachello. Dynamic symmetries at the critical Point. *Phys. Rev. Lett.* **85**, 3580 (2000).
2. F. Iachello. Analytic description of critical point nuclei in a spherical-axially deformed shape phase transition. *Phys. Rev. Lett.* **87**, 052502 (2001).
3. Z.P. Li, T. Nikšić, J. Mengt, G.A. Lalazissis, P. Ring. Beyond the relativistic mean-field approximation. III. Collective Hamiltonian in five dimensions. *Phys. Rev. C* **79**, 054301 (2009).
4. J. Kotila, K. Nomura, L. Guo, N. Shimizu, T. Otsuka. Shape phase transitions in the interacting boson model: Phenomenological versus microscopic descriptions. *Phys. Rev. C* **85**, 054309 (2012).
5. A.M. Khalaf, M.D. Okasha, G.S.M. Ahmed, A. Abdelsalam. Identical bands in doubly even nuclei in framework of variable moment of inertia (VMI) and interacting boson models. *Nucl. Phys. A* **997**, 121719 (2020).
6. R.F. Casten, N.V. Zamfir. Empirical realization of a critical point description in atomic nuclei. *Phys. Rev. Lett.* **87**, 052503 (2001)
7. E.A. McCutchan, N.V. Zamfir, R.F. Casten. Mapping the interacting boson approximation symmetry triangle: New trajectories of structural evolution of rare-earth nuclei. *Phys. Rev. C* **69**, 064306(2004).
8. D. Tonev, A. Dewald, T. Klug, P. Petkov, J. Jolie, A. Fitzler, O. Möller, S. Heinze, P. von Brentano, R.F. Casten. Transition probabilities in ^{154}Gd: Evidence for X(5) critical point symmetry. *Phys. Rev. C* **69**, 034334 (2004).
9. J.F. Zhang, J.L. Lu, B.H. Bai. Critical behaviour in nuclear structure from spherical to axially symmetric deformed shape in IBM. *Chin. Phys.* **16**, 1941 (2007).
10. E.A. McCutchan, N.V. Zamfir, R.F. Casten. Simple description of light W, Os, and Pt nuclei in the interacting boson model. *Phys. Rev. C* **71**, 034309 (2005).
11. N.V. Zamfir, E.A. McCutchan, R.F. Casten. The X(5) critical point nuclei and the interacting boson model symmetry triangle. *Phys. Atom. Nucl.* **67**, 1829 (2004).
12. J.B. Gupta. Role of $\gamma - g$ band mixing in triaxial vs. deformed nuclei. *Pramana – J. Phys.* **95**, 189 (2021).
13. S.Y. Lee, J.H. Lee. Electromagnetic properties in Samarium isotopes within the framework of the IBM-2. *J. Korean Phys. Soc.* **76**, 701 (2020).
14. M. Karday, H.M. Mittal, R. Mehra. Systematic study of rigid triaxiality in Ba-Pt nuclei and role of $Z = 64$ subshell effect. *Pramana – J. Phys.* **91**, 70 (2018).
15. M.R. Pahlavani, M.M. Dinan. Thermal properties of ^{172}Yb and ^{162}Dy isotopes in the back-shifted Fermi gas model with temperature-dependent pairing energy. *Pramana – J. Phys.* **93**, 37 (2019).
16. A. Arima, F. Iachello. Collective nuclear states as representations of a SU(6) group. *Phys. Rev. Lett.* **35**, 1069 (1975).
17. A. Arima, F. Iachello. Interacting boson model of collective nuclear states. II. The rotational limit. *Ann. Phys.* **111**, 201 (1978).
18. R.F. Casten, D.D. Warner. The interacting boson approximation. *Rev. Mod. Phys.* **60**, 389 (1988).
19. F.H. Al-Khudair, G.L. Long. Detailed description of mixed symmetry states in ^{94}Mo using interacting boson model. *Commun. Theor. Phys. (Beijing, China)*, **37**, 699 (2002).
20. F.H. Al-Khudair, G.L. Long, Y. Sun. Negative-parity states and β decays in odd Ho and Dy nuclei with $A = 151$, 153. *Phys. Rev. C* **77**, 034303 (2008).
21. A. Giannatiempo. Vibrational-γ bands in even $^{104-118}$Pd isotopes. *Phys. Rev. C* **98**, 034305 (2018).
22. G. Puddu, O. Scholten, T. Otsuka. Collective quadrupole states of Xe, Ba and Ce in the interacting boson model. *Nucl. Phys. A* **348**, 109 (1980).
23. F. Iachello, A. Arima. *The Interacting Boson Model* (Cambridge University Press, 1987).
24. F.H. Al-Khudair. Level structure of the Ge, Se, and Kr ($N = 52$, 53) isotopes within the framework of the interacting boson model. *Phys. Rev. C* **91**, 054304 (2015).
25. B. Decroix, C. De Coster, K. Heyde, A.M. Oros, J. De Beule. 1^+ mixed symmetry states and dipole transitions in the extended proton-neutron interacting boson model. *Phys. Rev. C* **58**, 232 (1998).
26. ENSDF. Nuclear data Sheet. (2023) http://www.nndc.bnl.gov/ensdf.
27. H. Qasim, F.H. Al-Khudair. Structure of the low-lying positive and negative parity states in even-even $^{144-154}$Nd isotopes. *Int. J. Mod. Phys. E* **28**, 1950107 (2019).
28. H. Qasim, F.H. Al-Khudair. Nuclear shape phase transition in even-even $^{158-168}$Hf isotopes. *Nucl. Phys. A* **1002**, 121962 (2020).
29. A.F. Barfield, J.L. Wood, B.R. Barret. Interacting boson model calculation of octupole states in deformed nuclei. *Phys. Rev. C* **34**, 2001 (1986).

30. C. Hart, D. Chuu, S. Hsieh H. Chiang. Negative-parity states of $N = 88$ isotones in the interacting boson approximation. *Phys. Lett. B* **163**, 295 (1985).
31. A. Arima, F. Iachello. Interacting boson model of collective states I. The vibrational limit. *Ann. Phys.* **99**, 253 (1976).
32. N. Minkov, S. Drenska, M. Strecker, W. Scheid, H. Lenske. Non-yrast nuclear spectra in a model of coherent quadrupole-octupole motion. *Phys. Rev. C* **85**, 034306 (2012).
33. J. Lange, K. Kumar, J.H. Hamilton. E0-E2-M1 multipole admixtures of transitions in even-even nuclei. *Rev. Mod. Phys.* **54**, 119 (1982).
34. K. Nomura, R. Rodriguez-Guzman, L.M. Robledo, J.E. Garcia-Ramos. Quadrupole-octupole coupling and the onset of octupole deformation in actinides. *Phys. Rev. C* **103**, 044311 (2021).
35. S. Kuyucak. Shape-phase transitions in mixed parity systems and the onset of octupole deformation. *Phys. Lett. B* **466**, 79 (1999).
36. S. Kuyucak, M. Honma. Mean field study of the quadrupole-octupole degree of freedom in the spdf boson model. *Phys. Rev. C* **65**, 064323 (2002).
37. K. Nomura, D. Vretenar, B.N. Lu. Microscopic analysis of the octupole phase transition in Th isotopes. *Phys. Rev. C* **88**, 021303(R) (2013).
38. K. Nomura, D. Vretenar, T. Niksic, B.N. Lu. Microscopic description of octupole shape-phase transitions in light actinide and rare-earth nuclei. *Phys. Rev. C* **89**, 024312 (2014).
39. J.N. Ginocchio, M. Kirson. An intrinsic state for the interacting boson model and its relationship to the Bohr-Mottelson model. *Nucl. Phys. A* **350**, 31 (1980).

Received 03.10.23

Х.Н. Касім, Ф.Х. Алъ-Худаїр

ДОСЛІДЖЕННЯ СТРУКТУРИ X(5)
У ПАРНО-ПАРНИХ ЯДРАХ РІДКІСНОЗЕМЕЛЬНИХ ЕЛЕМЕНТІВ Sm–Os В ОБЛАСТІ $N \approx 90$

Структура ротаційних смуг та форма ядер в області $N \approx 90$ досліджуються за допомогою моделі взаємодіючих бозонів. Досліджено енергетичні рівні та відношення енергій. Ми вивчали відношення $\delta E(J^-)/E(2_1^+)$ в залежності від масового числа для станів від $J^- = 1^-$ до $J^- = 11^-$. Було розраховано відношення $E(J_i^+)/E(2_1^+)$ енергій ротаційної смуги в залежності від кутового моменту (J_i^+). Ядра ^{152}Sm, ^{154}Gd та ^{160}Er мають обертальний SU(3) характер, тоді як ядра ^{156}Dy, ^{170}W та ^{176}Os виявляють характер X(5). Для дослідження еволюції форми побудовано графіки поверхні потенціальної енергії як функції β_2 та β_3. Отримані результати порівнюються з наявними емпіричними даними. Результати загалом добре узгоджуються для енергетичних спектрів, тоді як для інших величин маємо прийнятні результати або принаймні правильну загальну тенденцію.

Ключові слова: енергетичний рівень, симетрія критичної точки, бозонна модель, коефіцієнт змішування.